In Situ Remediation of Arsenic-Contaminated Groundwater by Injecting an Iron Oxide Nanoparticle-Based Adsorption Barrier

Sadjad Mohammadian [1], Hadi Tabani [2], Zahra Boosalik [2], Amir Asadi Rad [2], Beate Krok [1], Andreas Fritzsche [3], Kamal Khodaei [2,*] and Rainer U. Meckenstock [1,*]

[1] Environmental Microbiology and Biotechnology, University Duisburg-Essen, Universitätsstr. 5, 45141 Essen, Germany; sadjad.mohammadian@uni-due.de (S.M.); beate.krok@uni-due.de (B.K.)

[2] Department of Environmental Geology, Research Institute of Applied Sciences (ACECR), Shahid Beheshti University, Tehran 14155-4364, Iran; h_tabani@sbu.ac.ir (H.T.); zahra.boosalik@yahoo.com (Z.B.); engamirasadirad@gmail.com (A.A.R.)

[3] Institute of Geosciences, Friedrich-Schiller-University Jena, Burgweg 11, 07749 Jena, Germany; a.fritzsche@uni-jena.de

[*] Correspondence: khodaeik@yahoo.com (K.K.); rainer.meckenstock@uni-due.de (R.U.M.); Tel./Fax: +98-(21)-2243-1933 (K.K.); Tel.: +49-(0)-201-183-6601 (R.U.M.)

Abstract: Arsenic contamination of groundwater occurs due to both geogenic and anthropogenic processes. Conventional arsenic remediation techniques require extraction of groundwater into pump-and-treat systems, which are expensive and require long operational times. Hence, there is a need for cost-effective remediation. In this study, we assessed and validated the in situ remediation of arsenic contamination in groundwater resources using permeable reactive barriers (PRBs) made of injectable, colloidal iron oxide nanoparticles in the laboratory and in field-scale pilot tests. Sand-packed, flow-through column studies were used in order to assess the sorption behavior of the iron oxide nanoparticles using field materials (sand, groundwater) in the laboratory. The breakthrough curves were analyzed using a reactive transport model considering linear and nonlinear adsorption isotherms and were fitted best with a chemical nonequilibrium consideration. The results were used to design a pilot-scale field test. The injected 28 m^3 of nanoparticles (ca. 280 kg dry weight of iron oxide) were successfully delivered to the aquifer via an injection well. No mobile iron was detected downstream, confirming that a stable in situ barrier was formed that did not move with the groundwater flow. Arsenic concentrations in groundwater were reduced to the aimed 50% of the background value, despite the relatively short contact time between arsenic and the iron oxide in the barrier, due to the high flow velocity of 1.21 m/day. We compared the results of the laboratory and field tests and concluded that the single-parameter models based on retardation factor and/or adsorption capacity fail to predict the longevity of the barrier and the evolution of arsenic breakthrough with time, most likely because they do not consider the chemical nonequilibrium effects. Therefore, we propose that upscaling the laboratory findings to field design must be carried out with care and be coupled with detailed reactive transport models.

Keywords: arsenic; permeable reactive barrier (PRB); groundwater; in situ remediation; iron oxide nanoparticles

1. Introduction

Arsenic is a toxic heavy metalloid that can pose a variety of health risks to humans, such as skin problems and effects on the urinary or respiratory tracts [1,2]. The World Health Organization (WHO) includes arsenic as one of the ten chemicals of major public health concern and recommends a provisional limit for arsenic concentration of 10 μg/L [3,4] in drinking water supply resources. Arsenic contamination in water resources has been reported in different countries over the world [5], including Thailand [3], Croatia [6], India [7], Bangladesh [8], Mongolia and China [9,10], Mexico [11–13], the USA [14], and

Germany [15]. Therefore, there is a serious need to improve suitable technologies for treatment of arsenic-polluted water resources [16].

The metalloid arsenic occurs in more than 245 minerals [11,12] and shows distinct mobility in the environment [16]. Arsenic pollution may occur naturally from geological processes such as the weathering of rocks, volcanic emissions, and geothermal activities, or as a result of anthropogenic activities such as the production of semiconductors and the use of agricultural supplements such as pesticides and herbicides, or mining activities [17]. Arsenic can be found in a variety of forms in nature, of which, inorganic forms such as arsenate [As(V)] and arsenite [As (III)] are the most prevalent in groundwater [18,19]. As(V) is more mobile and toxic than As(III) and is more prevalent in anoxic waters at pH values between 6 and 8 [3,20–23]. Several technologies are used to remove arsenic from water including coagulation/filtration [24], membrane filtration [25], reverse osmosis, activated alumina, lime softening, adsorption [26], flushing with solvents and surfactant, steam treatment, phytoremediation, or ion exchange [27]. These techniques are used typically ex situ and in Pump&Treat systems, and require continuous extraction of groundwater during the entire remediation action, which could last several decades. This leads to extremely high operation and maintenance costs to keep arsenic levels below the recommended threshold values. In recent years, in situ remediation techniques using nanoparticles have been shown to be effective in removing contaminants from groundwater and at the same time reducing the costs of remediation actions [28–31]. In this approach, the reactive and/or adsorptive nanoparticles are injected into a plume of contaminant, where they spread and form a permeable reactive barrier (PRB) [28]. The nanoparticles cover the surface of sand grains in the aquifer and immobilize pollutants from the mobile phase (i.e., groundwater) through adsorption. Natural groundwater flow brings the contaminants into the PRB where they are removed from the water, and clean water leaves the PRB downstream. The PRB approach has many advantages over ex situ approaches, including avoiding aboveground infrastructure, reducing operation and maintenance costs, and applicability for deeper aquifers.

However, not all materials used in ex situ treatment can be adapted to in situ PRB treatment systems. According to Krok et al. [32], a substance must have special characteristics to be applicable for in situ remediation. It must be prepared in submicron or nanoscale colloidal form, so it can travel through small pores of the aquifer and reach a desired radius of influence (ROI) around the injection well. The colloids must remain as stable suspension and must not form aggregates; otherwise, they clog the pores. The substance must be nontoxic and nonharmful to micro-organisms and meiofauna in the aquifer. Most importantly, the substance used in PRBs must be adsorptive to provide a long-standing sink for contaminants [33]. Iron-based nanoparticles such as nZVI (nano zero-valent iron) and iron oxides (Goethite: α-FeOOH) have been proven efficient in the laboratory for removal of arsenic from contaminated groundwaters in batch and column studies [33–35]. In the case of nZVI, however, upscaling to the field is challenging. nZVI particles tend to aggregate, and their mobility in aquifers is limited [36,37]. Hence, large ROIs can be achieved only with high-pressure injection and fracking. In addition, nZVI is highly reactive and quickly oxidizes in water, resulting in the formation of hydrogen bubbles blocking pore space, which in turn diverts the groundwater flow away from PRB [38]. On the other hand, iron oxides such as Goethite (α-FeOOH) are abundant in aquifers and have low toxicity [39,40]. Goethite is the most stable iron oxyhydroxides and is produced by low-temperature oxidation of iron salts, most commonly iron sulfides. It has been shown that Goethite and Goethite-coated sand can effectively remove arsenic and mixtures of metals from aqueous media [34,35,41], constituting simple and inexpensive adsorbents for the removal of multiple pollutants [42]. Furthermore, Goethite nanoparticles have been shown to meet the abovementioned criteria for PRBs both in laboratory and field settings, forming homogeneous PRBS with ROIs larger than 2.5 m [29,32,34,43]. The previous field trials, however, focused on the removal of metal cations (Zn, Cu, Pd, ...) from contaminated groundwater in industrial sites with high contamination levels in the

mg/L range, while for arsenic the threshold values are typically much lower (10–50 µg/L). Montalvo and colleagues showed that the iron oxide nanoparticles used in this study reach this threshold both in batch and sand-packed columns [34,35].

This study aims to verify the applicability of iron oxide nanoparticles for remediating arsenic-contaminated drinking water resources using field materials and via field pilot testing. Therefore, the investigation carried out to assess the effectiveness and possible use of iron oxide PRBs for arsenic removal was divided into a laboratory and a field segment, coupled with reactive transport modeling. In the laboratory segment, the adsorption behavior of iron oxide nanoparticles was quantitatively assessed using groundwater and soil from an arsenic-contaminated aquifer. Reactive transport modelling was used to determine the effective parameters. In the field investigation segment, the iron oxide particles were injected into an aquifer to form a PRB. The arsenic concentrations downstream of the PRB were monitored for 210 days and the results were compared to the laboratory-driven predictions and modeling.

2. Methodology

This research was conducted in three segments, including laboratory testing, modeling, and field application. For the laboratory testing before field application, groundwater and soil samples were taken into the laboratory to obtain the site-specific adsorption capacity and adsorption behavior. Briefly, for both laboratory and field tests, Goethite nanoparticle batches of ca. 100 g/L were produced and diluted to the desired concentration before each test. The colloidal iron oxide nanoparticles used in this study were similar to those used in previous laboratory and field applications reported in [29,32]. In brief, the particles were synthesized following a modification of the method according to [44]. The particles consisted of Goethite as exclusive iron-(oxyhydr)oxide phase and were coated with humic acids for stabilization against aggregation (hydrodynamic size: 200–800 nm). The dispersions were stable for several months after synthesis. The stock dispersion had a Goethite content of ca. 100 ± 12 g per L and a pH of ca. 9.2. Previous studies showed that the iron oxide nanoparticles used in this study can adsorb >30 mg As per gram of Goethite nanoparticle both in batch and sand-packed columns using quartz sand [34,35]. Parameters affecting the mobility of these nanoparticles, and hence the expected radius of influence around the injection point, have been studied by [41,45]. Pilot [46] and field applications [29,32] showed that a radius of influence of >2.5 m can be achieved under real conditions in highly polluted industrial sites, and efficient removal of heavy metals was observed. The nanoparticles themselves contained no traces of arsenic.

2.1. Laboratory Test

In order to simulate the aquifer condition, sorption experiments in duplicates were carried out in Plexiglas columns packed with aquifer materials (total volume 23.5 mL, length of column 30 mm, porosity 0.34). Then, the sand-packed columns were flushed with groundwater from bottom to top. One pore volume (PV~8 mL) of iron oxide nanoparticle suspension at the concentration of ca. 5 g Goethite per liter was injected into the column using a peristaltic pump (Ismatec ICP8, Cole-Parmer, Wertheim, Germany) at a flowrate of 1 mL/min. Then, the pump was turned off to allow the iron oxide nanoparticles to deposit and cover the grain surface and form a permeable barrier. After 24 h, arsenic-containing groundwater was pumped through to the column at a flow rate of 1 mL/min, equivalent to a flow velocity of ca. 0.375 cm/min. The column effluent was collected using an autosampler (Omnicoll, Lambda, Brno, CZ) at ca. 3 PV intervals. The collected samples were analyzed using ICP-MS analysis (X-Series II, Thermo Fisher Scientific, Waltham, MA, USA). Prior to analysis, the samples were treated with HCl (37%, AnalaR NORMAPUR; VWR Prolabo, Darmstadt, Germany) and H_2O_2 (30%, Rotipuran; Carl Roth GmbH + Co KG, Karlsruhe, Germany) to completely dissolve any iron oxide nanoparticles that may have been potentially discharged from the column. In addition, the pH (Sentix 41; WTW, Weilheim, Germany) and electric conductivity (TetraCon 325; WTW, Weilheim, Germany)

were measured in untreated groundwater samples. A similar experiment without the addition of iron oxide nanoparticles was also performed and considered as a negative control.

2.2. Modeling

The adsorption column was modeled using a linear system form of the advection-dispersion equation (ADE) [47]. A two-site model with first-order kinetics was used to explain the adsorption of arsenic in Goethite-coated sands following [34,48]. This model assumes an equilibrium state at a fraction (*f*) of Goethite-coated sand, while nonequilibrium exists at the rest of the adsorption sites [49]. Using these assumptions, the ADE becomes:

$$\varepsilon\frac{\partial c}{\partial t} + q\frac{\partial c}{\partial x} + f\rho_b\frac{\partial S_1}{\partial t} + \alpha\rho_b\frac{\partial S_2}{\partial t} = \varepsilon D\frac{\partial^2 c}{\partial x^2} \tag{1}$$

where ε is the porosity of the medium [–], q is the Darcy velocity [L T^{-1}], c is the species concentration in the mobile phase [M L^{-3}], α is the first-order kinetic rate coefficient [T^{-1}], ρ_b is the bulk density of the solid matrix [M L^{-3}], and D is the dispersion coefficient [L^2 T^{-1}]. S_1 and S_2 are the concentrations in the solid phase at sites 1 and 2, for which, linear and nonlinear (Langmuir, Freundlich) isotherm models were considered:

$$S = \frac{K_D c^\beta}{1 + bc^\beta} \tag{2}$$

where b, β, and K_D are adsorption parameters. When $\beta = 1$, the above equation becomes the Langmuir isotherm; when $b = 0$, the equation becomes the Freundlich isotherm; and when both $\beta = 1$ and $b = 0$, it leads to a linear adsorption isotherm.

To obtain the in situ, site-specific adsorption nonequilibrium parameters (α, f, K_D, and either b or β, depending on adsorption isotherm), the experimental arsenic breakthrough results of the transport experiments were modeled using this model and using HYDRUS-1D [50]. Kinetic parameters were estimated from inverse data fitting and were compared to literature data.

Then, a simple one-dimensional linear model with a length of 10 m was built to simulate the field conditions in forward simulation mode. The obtained fitted parameters were applied to the first part (7.2 m) of the model where an adsorptive barrier using one injection point is installed (see below). No adsorption was assumed for the following 2.8 m. Breakthrough of arsenic at the downstream section (end of the model) was recorded and was then compared to real field data.

2.3. Field Application

2.3.1. Testing Site Area

The testing area (shown by the red box in Figure 1) is located at 36°34′59″ northern latitude and 47°15′44″ 50° eastern longitude in northwest Iran, near the Takht-e Soleymān, an archaeological site, and the city of Takab. The geology of the site includes alteration of marl and red sandstone. Various types of surficial quaternary sediment deposits (creamy white to light grey travertine) are present. Most common are unconsolidated stream alluvium and slope wash that resulted from hot springs activity during the Quaternary period. Arsenic-antimony-gold ores are prominent in the area with a mining history going back hundreds of years. Ancient and recent gold mine activities are one of the main sources of soil and water pollution. In addition, some metal(loid) contamination in the area is related to thermal and hot springs that are remnants of Quaternary volcanism. The hot springs originated from the circulation of meteoric water into the underlying layers, which subsequently rose to the surface.
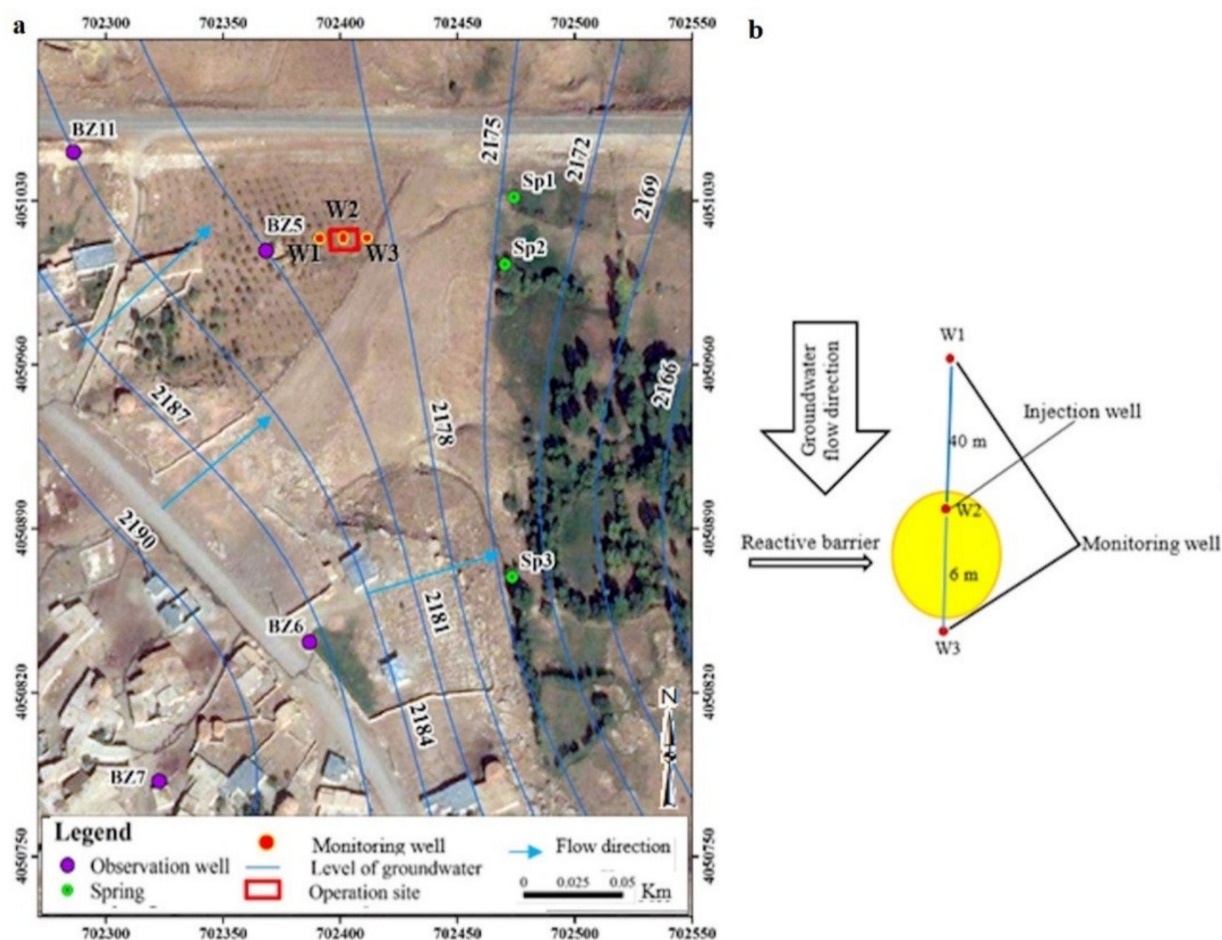
Figure 1. Top view of (**a**) the groundwater flow direction map of the site, and (**b**) the location of injection well and monitoring well in the testing area. The testing area is marked by the red square in the top part of Figure 1A. The springs are shown in green, and available observation wells are in red.

The groundwater flow direction in the testing area was to the northeast. The aquifer contains mainly coarse and medium sands with traces of silt and clays and an effective porosity of 15%. The water table was approximately 6.5 m below ground level, and the hydraulic gradient was about 6 percent. The aquifer of the testing area of the PRB contained coarse-grained sediments with high hydraulic conductivity of 3.5×10^{-5} m/s (determined by slug testing). This area is also affected by the groundwater divide line (Figure 1A), which has increased the groundwater velocity. The Darcy flux of ca. 0.18 m/day was calculated based on the measured hydraulic gradient and local hydraulic conductivities.

Arsenic concentrations were relatively stable during the year, with ca. 110 µg/L across the testing area. Barium and magnesium were other major elements found in the groundwater (Tables 1 and 2). Analysis of sediment samples revealed high sediment-bound concentrations of arsenic, barium, and especially manganese. Previous studies indicated the role of sediment-bound metals on the performance of PRBs and their effects on the lifetime of the installed barriers [29]. The sediment-bound metals compete with the metals in solution for the adsorption sites, and hence reduce the effective adsorption capacity of the iron oxides.

Table 1. Observed background metal concentrations in groundwater and aquifer sand.

Water/Sand	As	Ba	Cu	Mn	Zn	Al
Groundwater (µg/L)	110	112	<1	<1	6	120
Sand (mg/kg)	98	487	36	2299	98	6%

Table 2. Observed background physicochemical properties of the groundwater in the testing area.

Parameter/Ion Concentration	Temperature (°C)	pH	Conductivity (μS/cm)	K (mg/L)	Na (mg/L)	Mg (mg/L)	Ca (mg/L)
Average (std. deviation)	15.40 (7.41)	7.46 (0.44)	611 (351)	0.12 (0.2)	0.53 (0.92)	2.60 (2.10)	6.02 (7.42)
Min–Max	9.50–36.00	6.64–8.18	236–1284	(0.01–0.71)	0.04–3.11	0.28–8.48	1.55–30.05

2.3.2. Field Testing and Monitoring

The objective of the pilot field test was to quantitatively validate the application of iron oxide nanoparticles for in situ immobilization of arsenic in an in situ adsorption barrier. The remediation target was planned to be a 50%-reduction of the arsenic concentration in the groundwater. Since the size of the barrier was small compared to the total aquifer size, full remediation of the contaminated site was not a goal of this pilot test.

For implementing the in situ absorptive barrier, the iron oxide nanoparticle dispersion must be injected into the water-saturated aquifer. A pilot test was performed with one 12.5 m deep injection well cased with a 76 mm diameter slotted PVC pipe. A monitoring well (Figure 1b) was located 6 m downstream of the injection point to evaluate the efficiency of the adsorptive barrier. Furthermore, a natural spring was located ca. 15 m downstream of the barrier and was periodically sampled and analyzed.

Ca. 3000 L of concentrated iron oxide nanoparticles dispersion (ca. 100 g/L) were produced and transported from Germany to the site with a truck. During the injection, the concentrate was diluted on the site with tap water and a total of 28 m³ of the 1:10 diluted suspension (i.e., 10 g/L) were continuously injected into the saturated zone 8 m to 12.5 m below ground. The top of the groundwater surface was sealed with a pressure packer to ensure the delivery of the nanoparticles to the target depths. A pressure pump with an estimated flow rate of up to 18 L/min was used for injecting at low pressure (below 1.5 bar) to avoid hydraulic fracturing and/or daylighting.

The injection was carried out without any problem despite the cold weather during the application. Small fires were set close to the containers to reduce the risk of freezing the dispersion. No additional destabilizing agent was used because previous experience [32] showed that dilution of the nanoparticles in water will cause all nanoparticles to deposit within a short time (<24 h) [29,43].

Pre- and postapplication groundwater samples were taken from the indicated wells and were analyzed using ICP-MS to determine the concentration of dissolved metals in the groundwater.

3. Results and Discussion

3.1. Laboratory Testing Results

To mimic field conditions, adsorption tests were performed with sand-packed columns with or without iron oxide nanoparticle amendments. Figure 2a shows the relative effluent concentrations collected at different times, where the effluent arsenic concentrations (C_{out}) are normalized to the measured arsenic concentrations in untreated water (C_{in} = 110 μg/L). Without nanoparticles, arsenic broke through after 1–2 pore volumes (PVs) indicating that the natural adsorption capacity of the sand had already been saturated. In iron oxide-loaded columns, the effluent arsenic concentrations were lower compared to columns without nanoparticles, and slowly increased with time. Such behavior was also observed using similar nanoparticles by Montalvo et al. [34], who attributed this observation to nonequilibrium adsorption conditions.

The maximum site-specific adsorption capacity of the nanoparticles was calculated as 0.64 mg As/g nanoparticles by integrating the area between the two curves. This value is much lower than those reported in batch experiments (30 mg As/g nanoparticles, Montalvo et al. [34]) but is in agreement with observations that the effective adsorption capacity for arsenic is lower under flow-through conditions due to nonequilibrium [31]. At higher groundwater velocities, the contact time between the nanoparticles and the

dissolved arsenic is lower, which reduces the adsorption efficiency in comparison to batch experiments, where enough contact is provided by rigorous shaking over long times.
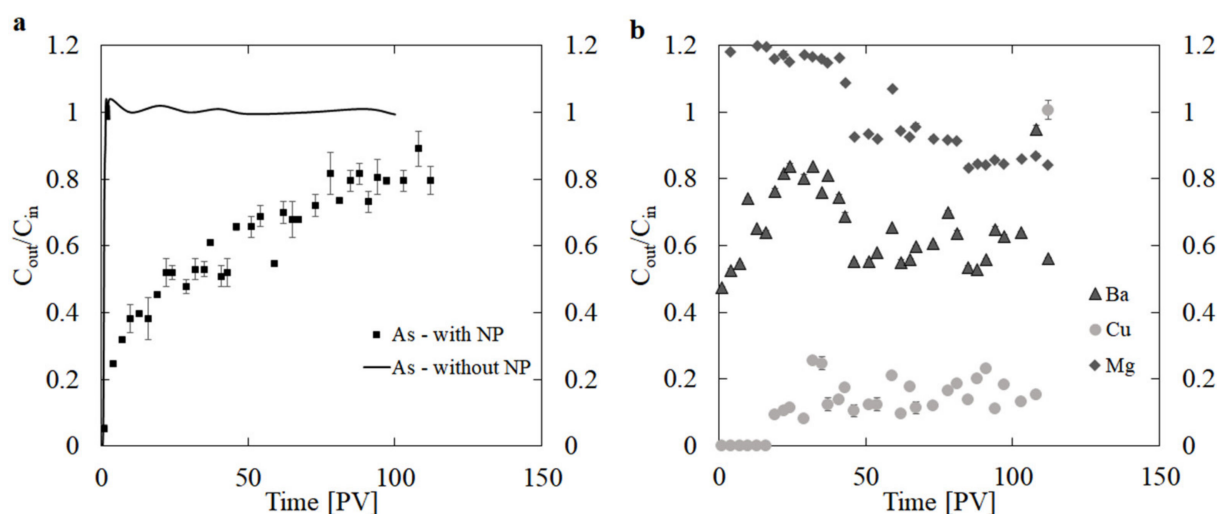

Figure 2. (**a**) Breakthrough curves for arsenic at velocity of 0.375 cm/min with and without addition of Goethite nanoparticles. Inlet concentration (C_{in}) was 110 μg arsenic per liter. The *x*-axis shows the time in pore volumes (PV), where 1 PV equals a contact time of 8 min. (**b**) Breakthrough curves for barium, copper, and magnesium during the same experiments. Data points and error bars depict means and standard deviations of arsenic concentrations from two experiments.

However, one should note the effect of water velocity on the adsorption efficiency. Montalvo et al. [34] observed that the effective adsorption capacity reduces at higher water velocities (16.2 mg/g at 0.0625 cm/min compared to 34.1 mg/g at 0.006 cm/min). The current study was carried out at a velocity of 0.375 cm/min, six times larger than the fastest velocity reported by [34]. Considering the effect of groundwater velocity, our results are in line with [34] and indicate the importance of the contact time in nonequilibrium sorption.

Another explanation for reduced adsorption capacity in comparison to batch experiments (ca. 30 mg/g, [34]) is the presence of other metallic ions in the groundwater and sediment (sand), which compete with arsenic for available sorption sites. Dissolved metals such as copper, barium, and magnesium compete with arsenic for adsorption sites, where copper has been shown to have higher affinity toward Goethite than arsenic [35]. Figure 2b confirms this assumption, where copper is highly retained ($C_{out}/C_{in} < 0.2$) throughout the experiment. The effluent magnesium concentrations exceeded that of the background value (2.6 mg/L), which is due to the fact that the injected Goethite-suspension contains traces of magnesium (1.0 mg/L), which is released from the column. Nevertheless, the outflow concentrations are below the threshold values of the Water Framework Directive (80 mg/L). Barium (background concentrations of 112 μg/L) is also adsorbed to Goethite and, as seen in Figure 2b, almost half of the incoming barium is retained by Goethite nanoparticles. Hence, we conclude that Goethite removes arsenic and copper more effectively than other metals, which is in agreement with [35]. In this study, the pH of groundwater (7.46) is higher than the point of zero charge for Goethite (pH_{ZPH} 6.9), and hence, adsorption of copper and other cations is promoted to the negatively charged Goethite surface, leading to smaller adsorption capacity for arsenic. Furthermore, previous studies [9] have indicated that the nanoparticles not only adsorb heavy metals and metalloids from the liquid phase (groundwater) but also adsorb the metals that are present in the sediment. The adsorption of metals from sand to the cover layer of iron oxide nanoparticles can be faster than from water since they are in direct contact with the nanoparticles. Although no further analysis was carried out in the current study, the effects of sediment-born metals such as barium and manganese on reducing the maximum adsorption capacity of iron oxides can be significant and should be considered.

3.2. Modeling Results

3.2.1. Inverse Fitting

Inverse fitting, using a two-site nonequilibrium model and with three adsorption isotherms, produced very good fits (Figure 3). This is in contrast with findings from [34], who reported only nonlinear models to correctly describe the adsorption of arsenic to Goethite. However, those experiments were carried out at much higher arsenic concentrations (1000–4500 µg/L), where the nonlinear behavior is expected due to saturation of adsorption sites. At lower concentrations, the linear segment of Langmuir and Freundlich isotherms is more pronounced. Kim et al. [48] performed batch adsorption experiments with concentrations similar to the present study (110 µg/L) and found good fits with linear and non-linear (Langmuir and Freundlich) isotherms models.
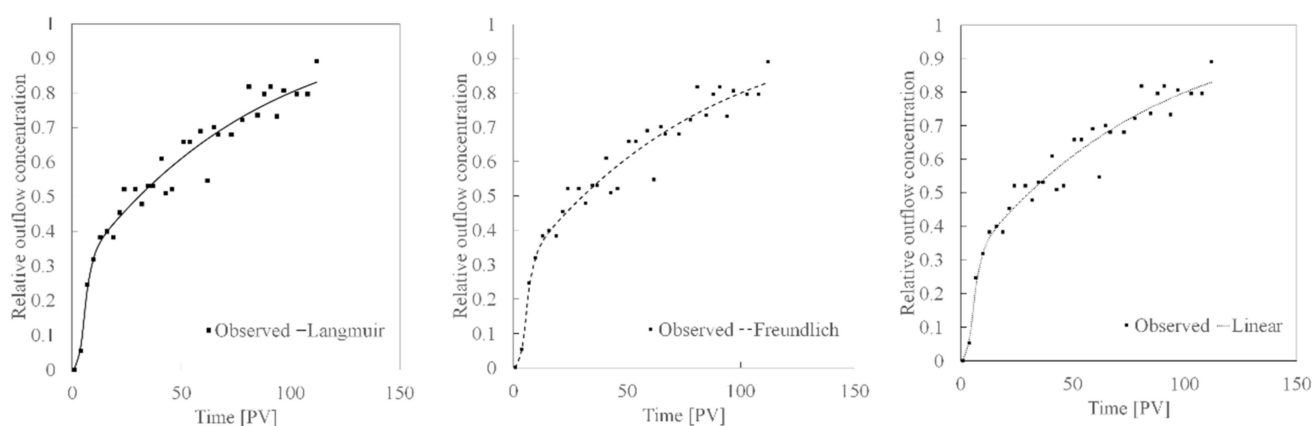

Figure 3. Fitted breakthrough curves using advection–dispersion equation considering two-site nonequilibrium model and Langmuir (**left**), Freundlich (**middle**), and linear (**right**) adsorption isotherms.

Table 3 summarizes the estimated parameters for the adsorption of arsenic onto Goethite-coated sand columns. The fitted parameters indicated that all models predicted only 13–14% of the adsorption sites in the equilibrium state and that nonequilibrium dominated the adsorption process (similar α). This relatively low fraction in equilibrium is most likely due to relatively high flow velocity in the column 0.375 cm/min, which reduces the residence time to reach equilibrium [51] and is in agreement with previous observations [32,34]. The value of adsorption isotherm coefficient K_D depends on the choice of the adsorption isotherm. For example, for Langmuir isotherms, it combines both the maximum adsorption efficiency and the affinity parameter [50], the latter represented here by parameter b. For linear isotherms, the K_D parameter represents the distribution coefficient and usually is used to determine the retardation factor, $R = 1 + K_D \rho_b / \varepsilon$, which explains the relative velocity of water to the velocity of arsenic [47]. Here, a retardation factor of 165.4 was calculated.

Table 3. Fitted chemical nonequilibrium transport parameters derived from the two-site model for the breakthrough curves and different adsorption isotherms shown in Figure 3. Parameters highlighted with * were predefined and not fitted.

Isotherm	f [–]	α [1/s]	K_D [m³/kg]	b [m³/kg]	β [–]
Linear	0.14	5.33×10^{-05}	3.28×10^{-02}	0 *	1 *
Langmuir	0.13	5.08×10^{-05}	3.60×10^{-02}	925	1 *
Freundlich	0.13	5.03×10^{-05}	1.52×10^{-02}	0 *	0.915

Note: Parameters highlighted with * were predefined and not fitted.

3.2.2. Forward Modeling

Using the fitted adsorption and nonequilibrium parameters, a predictive modeling of the simple field testing was performed using HYDRUS-1D and three adsorption isotherms (Figure 4). Simulations predicted earlier breakthroughs using linear isotherms in comparison to nonlinear isotherms for both injection and downstream wells. The rate constant parameter α is the largest for the linear model among the three adsorption models, which may lead to faster sorption and faster saturation of the adsorption sites and hence, slightly faster breakthrough [52]. The difference between the isotherms was more pronounced as the length of the simulated barrier increased, i.e., in the downstream wells the difference was larger than in the injection well.
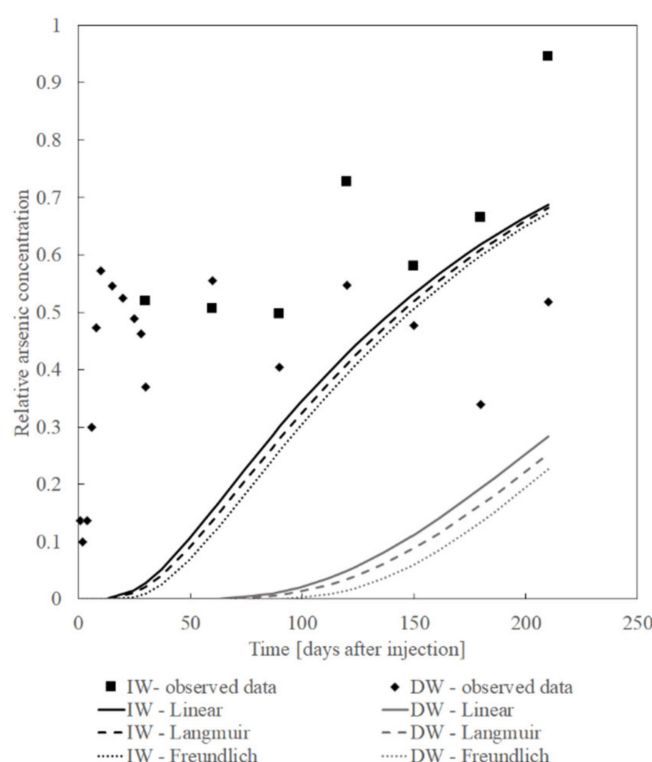
Figure 4. Comparison between observed arsenic concentrations at the injection (IW, black) and downstream (DW, grey) wells of the pilot site for different adsorption isotherms based on kinetic parameters from the column data (lines). The data points show the observed arsenic concentrations during field test.

3.3. Field Testing and Comparison to the Laboratory Data

A total of 28 m^3 of 1:10 diluted suspension (i.e., 10 g/L) were injected in the saturated zone (from 8 m to 12.5 m below ground level) in the injection well continuously. Based on the volumetric calculations and considering the local porosity of 15%, it was expected that these nanoparticles form a cylindrical barrier with a radius of 3.6 m under ideal conditions. Due to the high groundwater flow velocity (1.21 m/day) at the site, the barrier was probably a bit deformed and elongated in the direction of groundwater flow, and thinner in the perpendicular direction. The biggest influence on the shape of the barrier, however, has inhomogeneities in the hydraulic conductivity of the sediment which can lead to a preferential pumping of the injection fluid into higher conductive layers [46].

To form a stable, permeable barrier, it is very important that the injected nanoparticles remain at the site of injection and are not transported with the groundwater. Therefore, the iron concentration was measured in the downstream well and spring over four days after the injection. The maximum iron concentration of 8.5 mg/L was observed at day +1 in the downstream monitoring well, which was much lower than the injected nanoparticles'

suspension (ca. 10 g/L) (Figure 5). The iron concentrations dropped strongly on the next day and returned to the background value of < 1 mg/L on day three after injection, and then below the detection limit (up to 12 months monitoring, data not shown here). No increase in iron content was observed in the spring (15 m downstream of the barrier), which indicated that all injected nanoparticles were deposited near the injection point and were not transported with the groundwater flow.
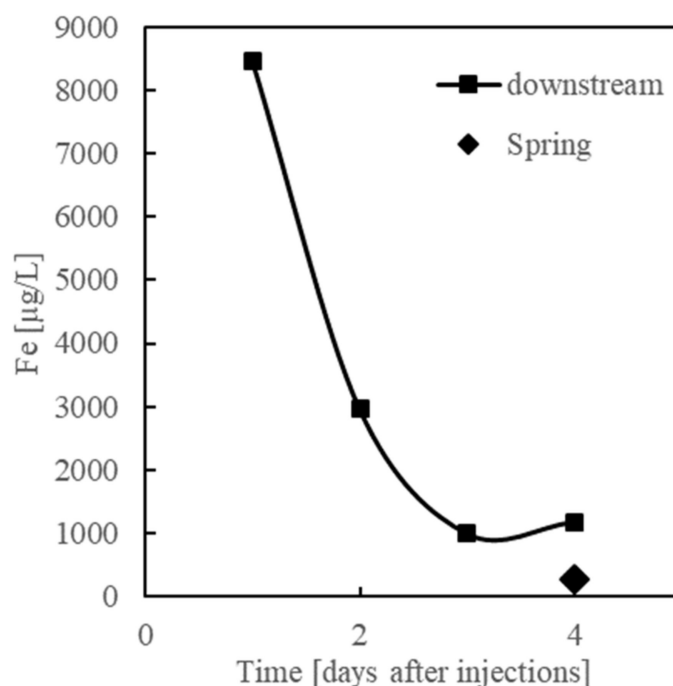

Figure 5. Observed iron concentrations in groundwater samples taken from the downstream well.

These results are in agreement with previous laboratory observations with metastable colloidal iron oxide nanoparticles [32,43], where no mobile iron oxide colloids were observed after 24 h in batch and column tests. In an earlier field study, Mohammadian et al. [29] similarly observed no increase in iron content downstream of the barrier after injection of iron oxide nanoparticles. In their study, the deposition of the nanoparticles near the injection well and within the radius of influence of 2.5 m was confirmed by taking sediment cores inside the barrier and measuring the elevated iron concentrations in the sediment. Hence, despite high groundwater flow velocity, the injected nanoparticles were not washed away and successfully deposited around the injection well.

Figure 6 shows the observed arsenic concentrations in injection and downstream wells up to seven months after the injection. The background concentrations remained relatively constant at 110 μg/L throughout the monitoring period and are shown using the red, dashed line. This value is higher than the regulatory threshold limits for arsenic, which are typically between 10 and 50 μg/L [3,4]. As mentioned, the aim of this study was to reduce the arsenic concentration in the testing area by 50% and quantitatively assess the performance of the installed barrier. Shortly after the injection, the arsenic concentrations in both injection and monitoring wells reduced from the original value of ca. 110 μg/L and stabilized after ca. 10 days around 50–60 μg/L. This ca. 50% reduction in arsenic concentration continued during almost the entire monitoring period of ca. seven months. Only in the last sampling point was the arsenic concentration in the injection well higher (ca. 104 μg/L). Another important observation was that the arsenic concentrations were almost always higher in the injection well than in the downstream monitoring well. This might be due to the shorter barrier length which the contaminated groundwater travelled through to the upstream part of the barrier from the inflow point to the injection well and, therefore, shorter contact time. The water sampled in the downstream monitoring well

passed through the entire extension of the barrier and had approximately twice the contact time compared to the water in the injection well.
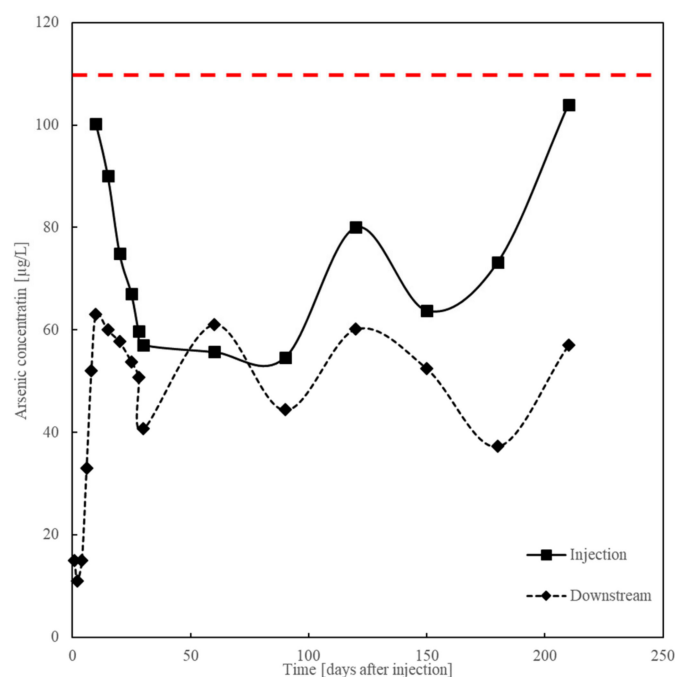

Figure 6. Observed arsenic concentrations in the injection and the downstream wells after injection of the iron oxide nanoparticles. Time 0 indicates the day of the injection.

3.4. Comparing Field Data with Lab Testing and Modeling

We performed laboratory experiments to simulate field conditions and calculate the performance and dimensions of the intended adsorption barrier in the field. Previous studies have shown that extrapolating batch adsorption and reaction studies alone are not sufficient and would introduce considerable uncertainty to the field application. The effective surface area of the nanoparticles is lower due to aggregation and deposition on the sediment during in situ application and, therefore, the available adsorption sites are less compared to batch studies [35,43]. Furthermore, the affinity of pollutants to the nanoparticles has been reported to be lower in nanoparticles-coated sand in comparison to the nanoparticles in batch experiments [34]. Therefore, sand-packed column studies and breakthrough curve analyses are essential to simulate the conditions occurring in real aquifers, including possible effects of sediments, flow conditions, and contact time. However, there are several approaches to interpret the breakthrough curves of sand-packed column studies and extrapolate the results to field applications. In this subsection, we review these approaches using our data and compare the results to the field observations.

The first approach is to calculate the adsorption capacity with the mass balance approach (area under the breakthrough curves). In the column experiments, the adsorption capacity of iron oxides was 0.64 mg arsenic per g of nanoparticles under geochemical conditions similar to the field. Assuming an ideal cylindrical barrier 7.2 m wide and 4.5 high, and the arsenic concentrations and groundwater flow measured at the site, 641.52 mg arsenic per day was flowing through the barrier. The total mass of nanoparticles injected (280 kg) was expected to retain, in total, 179.2 g arsenic. Accordingly, it would take ca. 279 days until the installed barrier is fully loaded with arsenic.

Another approach for extrapolating laboratory results to the field is based on the retardation factor. The calculated retardation factor in this study was 165.4. Considering a groundwater flow velocity of 1.21 m/day and the barrier length of 7.2 m, it would take ca. $t_{breakthrough} = \frac{l}{u_{arsenic}} = \frac{l}{u_{water}/R} = 981$ days before complete saturation of adsorption sites in the barrier.

Another approach is to use simplified reactive transport models such as those used in Section 3.2.2 of this study. Since nonequilibrium effects are also taken into account, the breakthrough is not sharp. Instead, the simulations showed that breakthrough occurred at ca. 100 days after injection and then the arsenic concentrations downstream continuously rose towards the background value. A long-time simulation (data not shown) resulted in a full saturation of the barrier after > 800 days.

By comparing this information to the observed arsenic concentrations after application of iron oxide nanoparticles in field testing (Figure 6), we validate their reliability to this case study. The field-testing data showed a relatively stable postinjection arsenic concentration of ca. 50–60 μg/L during the monitoring period in both observation points. None of the used approaches predict this trend exactly, but the reactive transport approach showed a slight increase in arsenic concentrations after day 25 in the injection well and day 100 in the downstream well. Generally, the single-parameter approaches (mass balance, retardation factor) inherently do not provide data about the evolution of concentrations during monitoring time before the breakthrough. Furthermore, they lack critical information about the nonequilibrium conditions. The mass balance approach resulted in a shorter barrier lifetime, which, considering the real field data, seems to be a more reliable approach than using the retardation factor. At the later phases of the monitoring period, the simulated data of the reactive transport model seemed to match better to the real field observations. At the earlier phases, disruptions due to the relatively large volume of the injected suspension, and hence, transient changes in aquifer conditions, were expected [29]. Furthermore, the intrusion of arsenic into the downstream well due to bypassing the barrier is very likely because of the relatively small size of the barrier. Following Krok et al. [32] who showed that the data from the middle of the barrier are more reliable for calibration and validation of the models, one can see that the simulation results predict the trend of the arsenic concentrations to a very good extent, especially at the injection point. An important point is that in the reactive transport model, we assumed a length of 3.6 m from the inlet to the injection point of the barrier (i.e., middle of the barrier), while in real field cases, the actual barrier length before this point might be less due to deformations occurring during the injection. Hence, the corresponding breakthrough curve will be shifted to an earlier time and a better match to the field data is expected.

3.5. Environmental Implications

A major aspect of designing an acceptable nanoremediation application for groundwater treatment, especially to water authorities and end-users, is the toxicity and side effects of the nanoparticles. The toxicology of the Goethite nanoparticles used in this study has been studied extensively for their effect on the environment or humans, and no toxic effects were found [39,40]. In addition, long-term studies have indicated that the adsorption PRBs installed are stable, and no remobilization or dissolution of iron oxide were observed even after strong changes in aquifer conditions [29]. The adsorbed pollutants also remain bound to iron oxide and are very unlikely to release [53], which makes them suitable as a long-term sink for groundwater contaminants such as arsenic.

4. Summary and Conclusions

Here, we assessed the applicability of nanoremediation for geogenic arsenic-contaminated groundwater resources via combining laboratory testing, numerical modelling, and a small-scale field test. The current study showed that all linear, Langmuir, and Freundlich isotherms were able to explain the adsorption behavior of arsenic to Goethite-coated sand at the concentration range used in this study. However, the results also showed that nonequilibrium effects must be taken into account while designing a field-scale nanoremediation application. We showed that the single-parameter extrapolation approaches, such as retardation factor or mass balance, fail to capture the nonequilibrium effects and hence may increase uncertainty in designing field applications [32,34]. The injected barrier decreased the arsenic concentration close to the drinking water threshold

values, which recommends the use of iron oxide nanoparticles for remediating arsenic-contaminated groundwater.

References

1. Bardach, A.E.; Ciapponi, A.; Soto, N.; Chaparro, M.R.; Calderon, M.; Briatore, A.; Cadoppi, N.; Tassara, R.; Litter, M.I. Epidemiology of chronic disease related to arsenic in Argentina: A systematic review. *Sci. Total Environ.* **2015**, *538*, 802–816. [CrossRef] [PubMed]
2. Nriagu, J.O. Arsenic in the environment (Part II, human health and ecosystem effects). In *Advances in Environmental Science and Technology*; John Wiley: New York, NY, USA, 1994.
3. WHO. *Arsenic and Arsenic Compounds Environmental Health Criteria 224*, 2nd ed.; World Health Organization: Geneva, Switzerland, 2001.
4. Kinniburgh, D.G.; Smedley, P. Arsenic contamination of groundwater in Bangladesh. In *British Geological Survey*; Department of Public Health Engineering: Dhaka, Bangladesh, 2001.
5. Alsayed, A.F.; Ashraf, M.A. Modified nanofiltration membrane treatment of saline water: A review. *Desalination Water Treat.* **2020**, *187*, 93–105. [CrossRef]
6. Ćavar, S.; Klapec, T.; Grubešić, R.J.; Valek, M. High exposure to arsenic from drinking water at several localities in eastern Croatia. *Sci. Total Environ.* **2005**, *339*, 277–282. [CrossRef] [PubMed]
7. Krishna, A.K.; Satyanarayanan, M.; Govil, P.K. Assessment of heavy metal pollution in water using multivariate statistical techniques in an industrial area: A case study from Patancheru, Medak District, Andhra Pradesh, India. *J. Hazard. Mater.* **2009**, *167*, 366–373. [CrossRef]
8. Von Ehrenstein, O.S.; Guha Mazumder, D.N.; Hira-Smith, M.; Ghosh, N.; Yuan, Y.; Windham, G.; Ghosh, A.; Haque, R.; Lahiri, S.; Kalman, D.; et al. Pregnancy Outcomes, Infant Mortality, and Arsenic in Drinking Water in West Bengal, India. *Am. J. Epidemiol.* **2006**, *163*, 662–669. [CrossRef]
9. Wade, T.J.; Xia, Y.; Wu, K.; Li, Y.; Ning, Z.; Le, X.C.; Lu, X.; Feng, Y.; He, X.; Mumford, J.L. Increased Mortality Associated with Well-Water Arsenic Exposure in Inner Mongolia, China. *Int. J. Environ. Res. Public Health* **2009**, *6*, 1107–1123. [CrossRef]
10. Xia, Y.; Wade, T.J.; Wu, K.; Li, Y.; Ning, Z.; Le, X.C.; Chen, B.; Feng, Y.; Mumford, J.L.; He, X. Well Water Arsenic Exposure, Arsenic Induced Skin-Lesions and Self-Reported Morbidity in Inner Mongolia. *Int. J. Environ. Res. Public Health* **2009**, *6*, 1010–1025. [CrossRef]
11. Smedley, P.L.; Kinniburgh, D.G. A review of the source, behaviour and distribution of arsenic in natural waters. *Appl. Geochem.* **2002**, *17*, 517–568. [CrossRef]
12. Mandal, B.K.; Suzuki, K.T. Arsenic round the world: A review. *Talanta* **2002**, *58*, 201–235. [CrossRef]
13. Armienta, M.A.; Segovia, N. Arsenic and fluoride in the groundwater of Mexico. *Environ. Geochem. Health* **2008**, *30*, 345–353. [CrossRef]
14. Yang, N.; Winkel, L.H.E.; Johannesson, K.H. Predicting Geogenic Arsenic Contamination in Shallow Groundwater of South Louisiana, United States. *Environ. Sci. Technol.* **2014**, *48*, 5660–5666. [CrossRef] [PubMed]
15. Banning, A. Geogenic arsenic and uranium in Germany: Large-scale distribution control in sediments and groundwater. *J. Hazard. Mater.* **2021**, *405*, 124186. [CrossRef] [PubMed]
16. Worou, C.N.; Chen, Z.-L.; Bacharou, T. Arsenic removal from water by nanofiltration membrane: Potentials and limitations. *Water Pract. Technol.* **2021**, *16*, 291–319. [CrossRef]
17. Fields, K.; Chen, A.; Wang, L. *Arsenic Removal from Drinking Water by Iron Removal Plants*; 45268; US EPA: Cincinnati, OH, USA, 2000.
18. Ferguson, J.F.; Gavis, J. A review of the arsenic cycle in natural waters. *Water Res.* **1972**, *6*, 1259–1274. [CrossRef]

19. Kanel, S.; Choi, H.; Kim, K.; Moon, S. Arsenic contamination in groundwater in Nepal: A new perspective and more health threat in South Asia. In *Natural Arsenic in Groundwater: Occurence, Remediation and Management*; Bundschuh, J., Bhattacharya, P., Chandrasekharam, D., Eds.; CRC: Boca Raton, FL, USA, 2005; pp. 103–108.

20. Nicomel, N.R.; Leus, K.; Folens, K.; Van Der Voort, P.; Du Laing, G. Technologies for Arsenic Removal from Water: Current Status and Future Perspectives. *Int. J. Environ. Res. Public Health* **2016**, *13*, 62. [CrossRef] [PubMed]

21. Sen, M.; Manna, A.; Pal, P. Removal of arsenic from contaminated groundwater by membrane-integrated hybrid treatment system. *J. Membr. Sci.* **2010**, *354*, 108–113. [CrossRef]

22. Uddin, M.T.; Mozumder, M.S.I.; Figoli, A.; Islam, M.A.; Drioli, E. Arsenic removal by conventional and membrane technology: An overview. *Indian J. Chem. Technol.* **2007**, *14*, 441–450.

23. Xia, S.; Dong, B.; Zhang, Q.; Xu, B.; Gao, N.; Causseranda, C. Study of arsenic removal by nanofiltration and its application in China. *Desalination* **2007**, *204*, 374–379. [CrossRef]

24. Ahmad, A.; Van De Wetering, S.; Groenendijk, M.; Bhattacharya, P. Advanced Oxidation—Coagulation—Filtration (AOCF)—An innovative treatment technology for targeting drinking water with <1 μg/L of arsenic. In Proceedings of the 5th International Congress on Arsenic in the Environment, Buenos Aires, Argentina, 11–16 May 2014; pp. 817–819.

25. Shih, M.-C. An overview of arsenic removal by pressure-drivenmembrane processes. *Desalination* **2005**, *172*, 85–97. [CrossRef]

26. Mohan, D.; Pittman, C.U., Jr. Arsenic removal from water/wastewater using adsorbents—A critical review. *J. Hazard. Mater.* **2007**, *142*, 1–53. [CrossRef]

27. Mondal, P.; Majumder, C.; Mohanty, B. Laboratory based approaches for arsenic remediation from contaminated water: Recent developments. *J. Hazard. Mater.* **2006**, *137*, 464–479. [CrossRef]

28. Blowes, D.W.; Ptacek, C.J.; Jambor, J.L. In-situ remediation of Cr (VI)-contaminated groundwater using permeable reactive walls: Laboratory studies. *Environ. Sci. Technol.* **1997**, *31*, 3348–3357. [CrossRef]

29. Mohammadian, S.; Krok, B.; Fritzsche, A.; Bianco, C.; Tosco, T.; Cagigal, E.; Mata, B.; Gonzalez, V.; Diez-Ortiz, M.; Ramos, V.; et al. Field-scale demonstration of in situ immobilization of heavy metals by injecting iron oxide nanoparticle adsorption barriers in groundwater. *J. Contam. Hydrol.* **2021**, *237*, 103741. [CrossRef]

30. McGregor, R. In Situ treatment of PFAS-impacted groundwater using colloidal activated Carbon. *Remediation* **2018**, *28*, 33–41. [CrossRef]

31. McGregor, R.; Vakili, F. The in situ treatment of BTEX, MTBE, and TBA in saline groundwater. *Remediation* **2019**, *29*, 107–116. [CrossRef]

32. Krok, B.; Mohammadian, S.; Noll, H.M.; Surau, C.; Markwort, S.; Fritzsche, A.; Nachev, M.; Sures, B.; Meckenstock, R.U. Remediation of zinc-contaminated groundwater by iron oxide in situ adsorption barriers—From lab to the field. *Sci. Total Environ.* **2022**, *807*, 151066. [CrossRef] [PubMed]

33. Lee, K.J.; Lee, Y.; Yoon, J.; Kamala-Kannan, S.; Park, S.M.; Oh, B.T. Assessment of zero-valent iron as a permeable reactive barrier for long-term removal of arsenic compounds from synthetic water. *Environ. Technol.* **2009**, *30*, 1425–1434. [CrossRef] [PubMed]

34. Montalvo, D.; Vanderschueren, R.; Fritzsche, A.; Meckenstock, R.U.; Smolders, E. Efficient removal of arsenate from oxic contaminated water by colloidal humic acid-coated goethite: Batch and column experiments. *J. Clean. Prod.* **2018**, *189*, 510–518. [CrossRef]

35. Montalvo, D.; Smolders, E. Metals and Metalloid Removal by Colloidal Humic Acid–Goethite: Column Experiments and Geochemical Modeling. *Vadose Zone J.* **2019**, *18*, 1–9. [CrossRef]

36. Tiraferri, A.; Chen, K.L.; Sethi, R.; Elimelech, M. Reduced aggregation and sedimentation of zero-valent iron nanoparticles in the presence of guar gum. *J. Colloid Interface Sci.* **2008**, *324*, 71–79. [CrossRef]

37. Ahn, J.-Y.; Kim, C.; Jun, S.-C.; Hwang, I. Field-scale investigation of nanoscale zero-valent iron (NZVI) injection parameters for enhanced delivery of NZVI particles to groundwater. *Water Res.* **2021**, *202*, 117402. [CrossRef] [PubMed]

38. Johnson, R.L.; Nurmi, J.T.; O'Brien Johnson, G.S.; Fan, D.; O'Brien Johnson, R.L.; Shi, Z.; Salter-Blanc, A.J.; Tratnyek, P.G.; Lowry, G.V. Field-Scale Transport and Transformation of Carboxymethylcellulose-Stabilized Nano Zero-Valent Iron. *Environ. Sci. Technol.* **2013**, *47*, 1573–1580. [CrossRef] [PubMed]

39. González-Andrés, V.; Diez-Ortiz, M.; Delpivo, C.; Janer, G.; Fritzsche, A.; Vázquez-Campos, S. Acute ecotoxicity of coated colloidal goethite nanoparticles on Daphnia magna: Evaluating the influence of exposure approaches. *Sci. Total Environ.* **2017**, *609*, 172–179. [CrossRef]

40. Cabellos, J.; González-Andrés, V.; Diez-Ortiz, M.; Janer, G. Iron oxide nanoparticle toxicity on human cell lines, aquatic and soil organisms and interactions with metal pollutants. *Toxicol. Lett.* **2018**, *295*, S209–S210. [CrossRef]

41. Mueller, B.; Dangol, B.; Ngai, T.K.K.; Hug, S.J. Kanchan arsenic filters in the lowlands of Nepal: Mode of operation, arsenic removal, and future improvements. *Environ. Geochem. Health* **2021**, *43*, 375–389. [CrossRef] [PubMed]

42. Hristovski, K.D.; Markovski, J. Engineering metal (hydr)oxide sorbents for removal of arsenate and similar weak-acid oxyanion contaminants: A critical review with emphasis on factors governing sorption processes. *Sci. Total Environ.* **2017**, *598*, 258–271. [CrossRef]

43. Tiraferri, A.; Saldarriaga Hernandez, L.A.; Bianco, C.; Tosco, T.; Sethi, R. Colloidal behavior of goethite nanoparticles modified with humic acid and implications for aquifer reclamation. *J. Nanoparticle Res.* **2017**, *19*, 107. [CrossRef]

44. Meckenstock, R.; Bosch, J. Method for the Degradation of Pollutants in Water and/or Soil. US8921091B2, 30 December 2014.

45. Bianco, C.; Patiño Higuita, J.E.; Tosco, T.; Tiraferri, A.; Sethi, R. Controlled Deposition of Particles in Porous Media for Effective Aquifer Nanoremediation. *Sci. Rep.* **2017**, *7*, 12992. [CrossRef]

46. Velimirovic, M.B.C.; Ferrantello, N.; Tosco, T.; Casasso, A.; Sethi, R.; Schmid, D.; Wagner, S.; Miyajima, K.; Klaas, N.; Meckenstock, R.U.; et al. A Large-Scale 3D Study on Transport of Humic Acid-Coated Goethite Nanoparticles for Aquifer Remediation. *Water* **2020**, *12*, 1207. [CrossRef]

47. Carrera, J.; Saaltink, M.W.; Soler-Sagarra, J.; Wang, J.; Valhondo, C. Reactive Transport: A Review of Basic Concepts with Emphasis on Biochemical Processes. *Energies* **2022**, *15*, 925. [CrossRef]

48. Kim, L.; Thanh, N.T.; Toan, P.V.; Minh, H.V.T.; Kumar, P. Removal of Arsenic in Groundwater Using Fe(III) Oxyhydroxide Coated Sand: A Case Study in Mekong Delta, Vietnam. *Hydrology* **2022**, *9*, 15. [CrossRef]

49. Selim, H.M.; Ma, L.; Zhu, H. Predicting Solute Transport in Soils Second-Order Two-Site Models. *Soil Sci. Soc. Am. J.* **1999**, *63*, 768–777. [CrossRef]

50. Šimůnek, J.; van Genuchten, M.T. Modeling Nonequilibrium Flow and Transport Processes Using HYDRUS. *Vadose Zone J.* **2008**, *7*, 782–797. [CrossRef]

51. Stolze, L.; Rolle, M. Surface complexation reactions in sandy porous media: Effects of incomplete mixing and mass-transfer limitations in flow-through systems. *J. Contam. Hydrol.* **2022**, *246*, 103965. [CrossRef] [PubMed]

52. Ghorai, S.; Pant, K.K. Equilibrium, kinetics and breakthrough studies for adsorption of fluoride on activated alumina. *Sep. Purif. Technol.* **2005**, *42*, 265–271. [CrossRef]

53. Mollenkopf, M.; Fritzsche, A.; Montalvo, D.; Diez-Ortiz, M.; González-Andrés, V.; Smolders, E.; Meckenstock, R.; Totsche, K.U. Exposure of humic acid-coated goethite colloids to groundwater does not affect their adsorption of metal(loid)s and their impact on Daphnid mobility. *Sci. Total Environ.* **2021**, *797*, 149153. [CrossRef] [PubMed]